Mutation-driven modulation of GPCR pharmacology in cancer: insights from adenosine and serotonin receptors

Feng, C.

Chapter 3

Effects of cancer-associated mutations of the adenosine $A_{2A}AR$ on ligand binding affinity and receptor function

Chenlin Feng, Xuesong Wang, Willem Jespers, Rongfang Liu, Sofía Denise Zamarbide Losada, Marina Gorostiola González, Gerard J. P. van Westen, Erik H. J. Danen, Laura H. Heitman

Adapted from: *Molecules*. 2022 Jul 22;27(15):4676

Abstract

The adenosine A_{2A} receptor (A_{2A}AR) is a class A G protein-coupled receptor (GPCR). It is an immune-checkpoint in the tumor micro-environment and has become an emerging target for cancer treatment. In this study, we aimed to explore the effects of cancer patient-derived A_{2A}AR mutations on ligand binding and receptor function. Wild-type A_{2A}AR and 15 mutants identified by Genomic Data Commons (GDC) in human cancers were expressed in HEK293T cells. Firstly, we found that the binding affinity for the agonist NECA was decreased for six mutants, but increased for the V275A mutant. Mutations A165V and A265V decreased the binding affinity of the antagonist ZM241385. Secondly, we found the potency of NECA (EC50) in an impedance-based cell morphology assay was mostly correlated with the binding affinity for the different mutants. Moreover, S132L and H278N were found to shift the A_{2A}AR towards the inactive state. Importantly, we found that ZM241385 could not inhibit the activation of V275A and P285L stimulated by NECA. Taken together, cancer-associated mutations of A_{2A}AR modulate ligand binding and receptor function. This study provides fundamental insights in the structure-activity relationship of A_{2A}AR and provides insights for A_{2A}AR-related personalized treatment in cancer.

1. Introduction

The adenosine A_{2A} receptor (A_{2A}AR), together with the other three subtypes of adenosine receptors (A_1AR, A_{2B}AR, A_3AR), belong to class A G protein-coupled receptors (GPCRs) [1]. As common features of GPCRs, A_{2A}AR has an extracellular N-terminal, seven trans-membrane helices (TM1-TM7) connected by three intracellular loops (ICL1-ICL3) and three extracellular loops (ECL1-ECL3), and an intracellular C-terminal [2]. When stimulated by its endogenous agonist adenosine or blocked by exogenous antagonists caffeine and theophylline, the A_{2A}AR is involved in many physiological and pathological activities, including neurotransmission, blood flow regulation, inflammation, and cancer [3].

The role of A_{2A}AR in cancer development has raised much interest in recent years, which is highlighted by its immunosuppressive effects in the tumor micro-environment (TME). Adenosine is normally present at very low extracellular levels in healthy tissue [4]. While in the TME, high levels of adenosine are present because more ATP is secreted by cell damage and hypoxia, which is further metabolized to AMP and adenosine [5]. Activation of A_{2A}AR on immune cells was found to suppress their anti-tumor responses, such as inhibition of CD8+ T cell activity [6], inhibition of antigen presentation by dendritic cells [7], and suppression of cytotoxic function of NK cells [8]. Several *in-vivo* studies have demonstrated the potential of small molecule inhibitors as well as blocking antibodies targeting A_{2A}AR to treat cancer [9-11]. Thus, A_{2A}AR is an emerging immune check-point and a promising target for cancer-treatment [12].

Hitherto, several crystal structures of A_{2A}AR in complex with either an agonist or antagonist have been resolved [13-15]. However, most knowledge on structure and function of A_{2A}AR, as well as drug discovery, is based on the wild-type receptor. Mutagenesis studies have been widely performed for A_{2A}AR and many other GPCRs, where residues in the ligand binding site were often replaced by alanine to identify key interactions of ligands with wild-type receptor [16, 17]. In previous research conducted in our group, we also used mutagenesis experiments to reveal the mechanism of antagonist dissociation from A_{2A}AR [18, 19]. Nevertheless, we still lack knowledge on ligand binding and function of mutant A_{2A}ARs, especially when these mutations occur in physiological conditions as natural variants or in pathological conditions as potential disease-driving factors. As for cancer, nearly 20% of human tumors contain mutations in genes encoding GPCRs [20], and many genes are statistically more frequently mutated relative to the background mutation rate [21]. Therefore, further investigation on cancer-associated mutations would help to better understand the phenotypical and biological outcome of these mutations and could promote personalized drug discovery.

In this study, by exploring the sequencing data from Genomic Data Commons Data Portal (GDC), we selected 15 A_{2A}AR mutations found in cancer tissue and investigated their effects on ligand binding and receptor function. Our results showed that six mutations decreased the binding affinity of agonist NECA compared to wild-type A_{2A}AR, while only one mutation increased the affinity. Two mutations were found to decrease the affinity of antagonist ZM241385. Besides, several mutations could alter the potency of NECA on receptor activation (EC50) or ZM241385 on receptor inhibition (IC50), mostly correlated with changes in binding affinity. This study is the first to systematically characterize cancer-associated mutations of A_{2A}AR, and pinpoints mutations that impact on receptor activity and that may influence therapeutic strategies targeting A_{2A}AR.

2. Results

2.1. Selection of cancer-associated A_{2A}AR mutations

From the Genomic Data Commons database (version 22.0, as collected by Bongers *et al*.) [22, 23], in total 58 A_{2A}AR single-site missense mutations were identified in patients of different cancer types. As shown in **Figure 3.1**, these mutations were distributed all over the receptor. Among them, 15 mutations were located towards the extracellular region, as seen from the most conserved *.50 residues (in Ballesteros–Weinstein numbering system) [24], and the other mutations were at the lower part of the receptor. Since most A_{2A}AR agonists and antagonists are extracellular ligands, it was inferred that mutations at the upper part were relatively close to the binding pocket and potentially involved in ligand binding or entry. Therefore, these 15 mutations were selected for further investigation. Of note, A265T^{ECL3} and S281L$^{7.46}$ have also been identified as natural variants (The 1000 Genomes Project Consortium, as collected by Bongers *et al*.) [23, 25], while the other mutations could be considered cancer specific (**Table S3.1**).

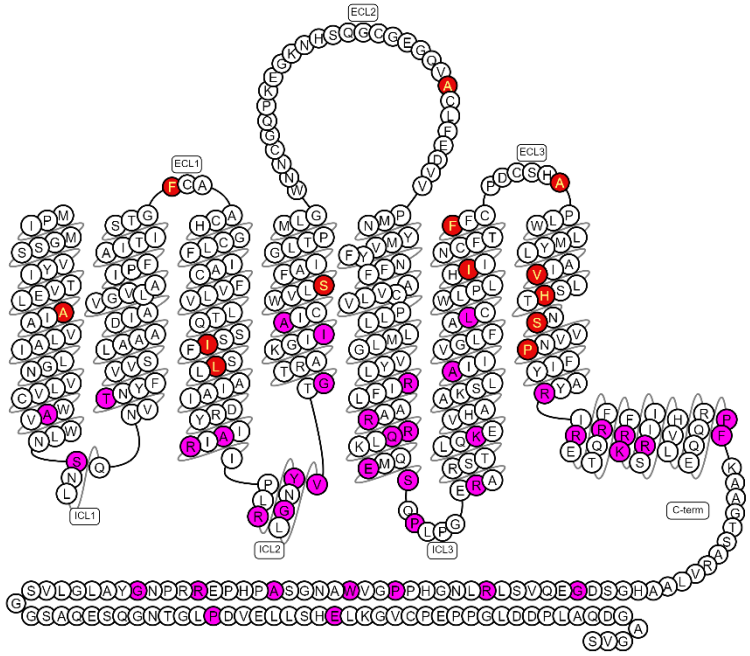

Figure 3.1. Snake-plot showing the primary structure of wild-type human A_{2A}AR. Red: residues with cancer-associated mutations at upper part of the receptor; Magenta: residues with cancer-associated mutations at lower part of the receptor.

2.2. Validation of expression and radioligand binding at wild-type and mutant A_{2A}ARs

To validate the expression and radioligand binding ability of A_{2A}ARs, 2.5 nM [^{3}H]ZM241385 was first applied for wild-type and 15 mutant receptors of interest. The binding window was defined as the difference between total binding (TB) and non-specific binding (NSB), thus representing specific binding of the radioligand at the (mutant) A_{2A}ARs. As shown in **Figure 3.2A**, [^{3}H]ZM241385 did not bind specifically to HEK293T membranes transfected with empty plasmid (mock), indicating that the endogenous expression of A_{2A}AR was negligible comparing to A_{2A}AR overexpressed by transfection. All mutants displayed a lower specific binding of [^{3}H]ZM241385 than the wild-type receptor, which suggested that they either had a lower expression level or [^{3}H]ZM241385 bound to them with lower affinity. Of note, especially for

S132L, H278N, S281L and P285L mutants, a significantly decreased binding by [^{3}H]ZM241385 was observed.

With a N-terminal FLAG-tagged construction of the overexpressed receptors, ELISA was performed to determine the expression level of the 4 mutants that displayed the lowest radioligand binding capacity, as shown in **Figure 3.2B**. The average expression level of wild-type A_{2A}AR was significantly higher (~2.8 fold) than mock HEK293T cells, while the expression level of all 4 mutants was not significantly different from mock. These results indicated that the low expression of S132L, H278N, S281L and P285L might be the main reason why little binding of [^{3}H]ZM241385 was observed. Consequently, the affinity of ZM241385 and NECA could not be determined for these mutants.

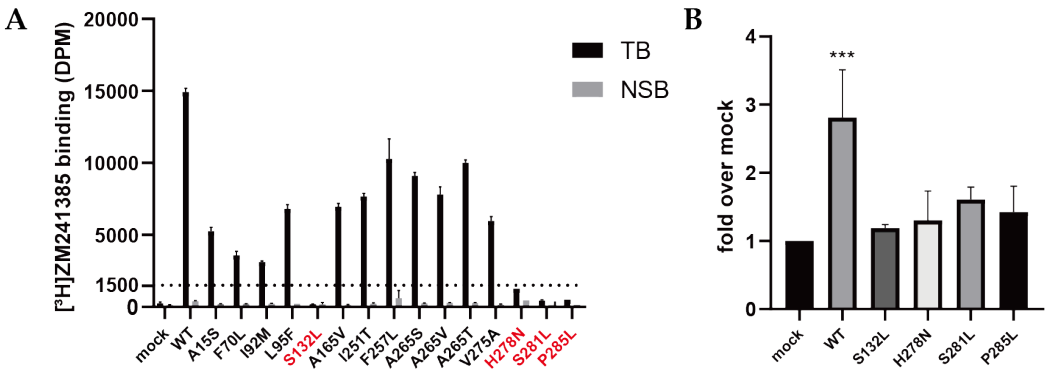

Figure 3.2. Radioligand binding capacity and expression of wild-type and mutant A_{2A}ARs. (**A**) Radioligand binding of 2.5 nM [^{3}H]ZM241385 with 10ug membrane protein of HEK293T cells transiently transfected with wild-type or mutant A_{2A}AR. Specific binding was defined as the difference between total binding (TB) and non-specific binding (NSB). NSB was determined with 100 μM NECA as displacer. Mutants of which the specific binding of 2.5 nM [^{3}H]ZM241385 lower than 1000 dpm were labeled red. Data are shown as mean ± SD of two independent experiments performed in duplicate. (**B**) Expression level of transiently transfected WT and mutant A_{2A}ARs on HEK293T cell membrane, measured by enzyme-linked immunosorbent assay. Data are shown as mean ± SD of two independent experiments performed in quintuplicate. (*P <0.05, **P <0.01, ***P <0.001, ordinary one-way ANOVA with Dunnett's multiple comparisons test, mock as control).

2.3. Quantification of expression level (B_{max}) and ZM241385 binding affinity (K_D) for A_{2A}ARs

Radioligand homologous displacement experiments were performed to determine the affinity of ZM241385 and the receptor expression level for wild-type and 11 mutant A_{2A}ARs (**Table 3.1**). It was shown that ZM241385 bound to A165V (K_D=2.2 nM, **Figure 3.3B**) and A265V (K_D=3.1 nM, **Figure 3.3C**) with a lower affinity than wild-type receptor (K_D=0.98 nM, **Figure 3.3A**). While the pK_D for the other 9 mutants were not significantly different from wild-type (**Figure 3.3D** and **Figure S3.1**), indicating that these mutations did not affect the binding affinity of ZM241385 ($p > 0.05$, ordinary one-way ANOVA).

The expression level of A_{2A}ARs in transiently transfected HEK293T cells was presented as B_{max} (**Table 3.1**). Although all mutants were expressed at high levels after transient transfection, 7 mutants showed significantly lower expression level compared to wild-type A_{2A}AR (B_{max} = 37 pmol/mg), i.e., A15S (12 pmol/mg, **Figure 3.3D**), F70L (8 pmol/mg), I92M (9 pmol/mg), L95F (10 pmol/mg), A165V (17 pmol/mg), I251T (14 pmol/mg), and V275A (20 pmol/mg). The

other 4 mutants (F275L, A265S, A265V, A265T) showed similar expression levels to wild-type receptor.

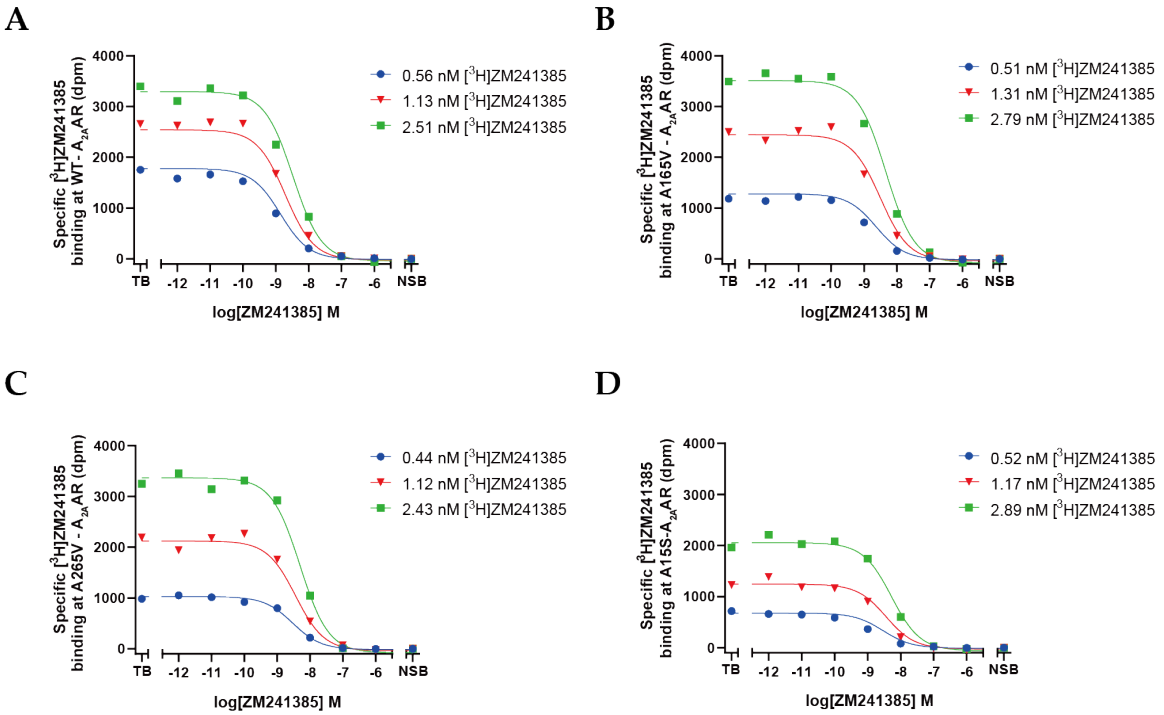

Figure 3.3. Homologous displacement of three concentrations of [^{3}H]ZM241385 by increasing concentrations of ZM241385 at WT-A_{2A}AR (**A**), A165V-A_{2A}AR (**B**), A265V-A_{2A}AR (**C**) and A15S-A_{2A}AR (**D**). Note that different concentrations of membranes were used dependent on receptor expression levels, i.e. WT-A_{2A}AR (1 µg), A165V-A_{2A}AR (3 µg), A265V-A_{2A}AR (1.5 µg) and A15S-A_{2A}AR (3 µg). Representative curves from one experiment performed in duplicate. Compared to WT-A_{2A}AR, A165V and A265V displayed different affinity with ZM241385, and A15S displayed similar affinity but different B_{max}. Graphs for other mutants can be found in **Figure S3.1**.

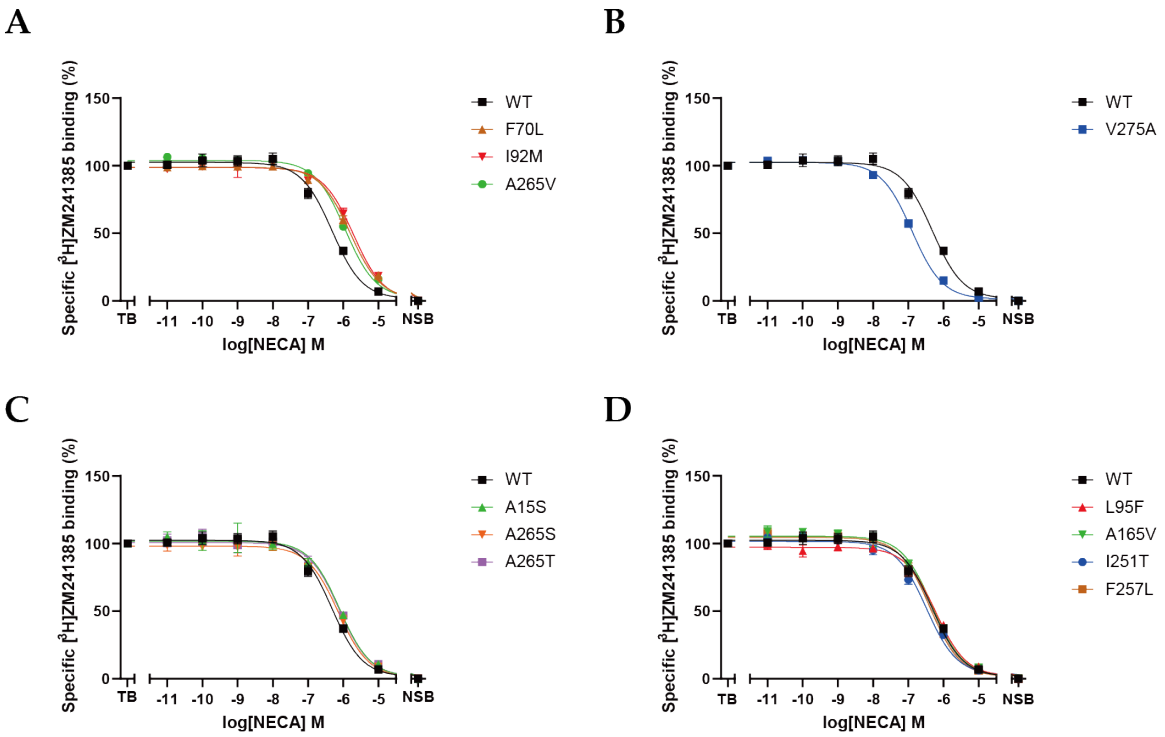

Figure 3.4. Displacement of [^{3}H]ZM241385 by increasing concentrations of NECA at wild-type and mutant A_{2A}ARs. Compared to wild-type A_{2A}AR, three mutants displayed lower affinity with NECA (**A**), V275A-A_{2A}AR displayed higher affinity with NECA (**B**), three mutants displayed slightly different affinity with NECA (**C**), and four mutants displayed similar affinity with NECA (**D**). Data are shown as mean ± SEM of three independent experiments each performed in duplicate.

Table 3.1. Affinity values of ligands at the wild-type (WT) and mutant A_{2A}ARs and their expression level (B_{max}).

Mutant	ZM241385	NECA	B_{max} [a]
	pK_D [a] (K_D (nM))	pK_i [b] (K_i (nM))	(pmol/mg)
WT	9.0 ± 0.1 (0.98)	6.9 ± 0.0 (134)	37 ± 5
A15S$^{1.41}$	8.9 ± 0.1 (1.5)	6.6 ± 0.1** (277)	12 ± 2****
F70L^{ECL1}	8.8 ± 0.1 (1.7)	6.2 ± 0.1**** (595)	8 ± 1****
I92M$^{3.40}$	8.9 ± 0.1 (1.3)	6.2 ± 0.1**** (606)	9 ± 1****
L95F$^{3.43}$	9.1 ± 0.0 (0.83)	6.9 ± 0.1 (144)	10 ± 1****
A165V^{ECL2}	8.7 ± 0.1** (2.2)	6.7 ± 0.0 (210)	17 ± 1***
I251T$^{6.53}$	8.8 ± 0.1 (1.9)	6.9 ± 0.1 (134)	14 ± 1***
F257L$^{6.59}$	8.8 ± 0.0 (1.8)	6.8 ± 0.0 (151)	27 ± 1
A265S^{ECL3}	8.9 ± 0.0 (1.3)	6.6 ± 0.1* (246)	27 ± 6
A265V^{ECL3}	8.5 ± 0.1*** (3.1)	6.2 ± 0.0**** (632)	39 ± 1
A265T^{ECL3}	8.9 ± 0.0 (1.2)	6.6 ± 0.0** (266)	37 ± 6
V275A$^{7.40}$	8.9 ± 0.1 (1.4)	7.4 ± 0.0**** (42)	20 ± 2**

[a] pK_D and B_{max} were determined by homologous displacement assay, where three concentrations of [^{3}H]ZM241385 were displaced by increasing concentrations of ZM241385. [b] pKi values were determined by heterologous displacement assay, where [^{3}H]ZM241385 was displaced by increasing concentrations of NECA. Values for S132L$^{4.53}$, H278N$^{7.43}$, S281L$^{7.46}$, P285L$^{7.50}$ were not determined because little binding of [^{3}H]ZM241385 was observed. Data are represented as Mean ± SEM of three independent experiments performed in duplicate. (Significant difference from wild-type was shown as *P <0.05, **P <0.01, ***P <0.001, ordinary one-way ANOVA with Dunnett's multiple comparisons test).

2.4. Quantification of NECA binding affinity (K_i) for A_{2A}ARs

The binding affinity of NECA at the wild-type and 11 mutant A_{2A}ARs were determined with radioligand heterologous displacement experiments. Based on the results shown in **Figure 3.4A** and **Table 3.1**, F70L (K_i=595 nM), I92M (K_i=606 nM), and A265V (K_i=632 nM) drastically decreased the binding affinity of NECA compared to wild-type A_{2A}AR (K_i=134 nM). Besides, A15S, A265S and A265T slightly but significantly decreased the binding affinity of NECA by approximately 2-fold (**Figure 3.4C**). Interestingly, V275A (K_i=42 nM, **Figure 3.4B**) was the only mutation that increased the affinity of NECA for the A_{2A}AR.

2.5. Functional effects of cancer-associated mutations on A_{2A}AR in a label-free whole cell assay

To investigate the functional consequence of A_{2A}AR mutations, HEK293T cells transiently transfected with either wild-type or mutant A_{2A}ARs were used in the cell morphology assay. In total eight mutants were selected for functional characterization, as these mutants either displayed over 3-fold change in binding affinity of NECA (F70L, I92M, A265V, V275A) or could not be assessed in binding experiments due to their low expression levels (S132L, H278N, S281L, P285L; **Figure 3.2**). For the first set of four mutants, ELISA experiments were also performed, and the results indicated that they were successfully expressed with similar levels to the wild-type A_{2A}AR (**Figure 3.5A**).

Next, the changes in cell morphology were monitored in real time after stimulation of the cells with the agonist NECA for wild-type and the selected eight mutants. It is shown in **Figure 3.5B** that the cell index (CI) of wild-type A_{2A}AR transfected cells slightly decreased upon addition of NECA, then sharply increased and reached a peak response within 10~15 minutes. Where after, the CI gradually decreased towards a plateau within 60 min, and continued to decrease slowly towards baseline levels. The NECA-induced response was dose-dependent (**Figure 3.5B**), and resulted in a potency of 8.4 ± 0.2 for wild-type A_{2A}AR (**Table 3.2**).

Having established a wild-type A_{2A}AR response for NECA in transiently transfected HEK293T cells, the eight mutants above were characterized following the same procedure. All eight mutants could be activated by NECA, resulting in a similar CI trace shape as for wild-type receptor (data not shown). The potency (EC_{50}), intrinsic efficacy (E_{max}) and relative efficacy (τ) of NECA for each A_{2A}AR mutant were determined and detailed in **Table 3.2**. NECA displayed a significantly decreased potency for almost all mutants when compared to wild-type A_{2A}AR (pEC_{50} = 8.4 ± 0.2), except for F70L (pEC_{50} = 7.6 ± 0.2) and S281L (pEC_{50} = 7.7 ± 0.3), for which the potencies were modestly decreased but not statistically different ($p > 0.05$, ordinary one-way ANOVA). Notably, V275A, the only mutant with an increased binding affinity for NECA (**Table 3.1**), displayed the lowest potency (pEC_{50} = 7.1 ± 0.1). Moreover, S132L and H278N, which had much lower expression levels than the wild-type receptor (Fig 2B), both showed a significant increase of efficacy (E_{max}% = 248 ± 30 for S132L, E_{max}% = 223 ± 33 for H278N, E_{max}% = 100 ± 5 for WT). The intrinsic efficacy for other mutants was not significantly different from

that at the wild-type receptor. The relative efficacy was also calculated for each mutant receptor, where the affinity of NECA is taken into consideration. This resulted in a different ranking of NECA at the different receptors compared to the intrinsic efficacy (**Table 3.2**). The wild-type A_{2A}AR showed the highest relative efficacy (τ = 37 ± 13), followed by F70L (τ = 28 ± 11), A265V (τ = 21 ± 8) and I92M (τ = 10 ± 3), while V275A (τ = 1 ± 0) showed the lowest relative efficacy, indicating that this mutation causes a loss in coupling efficiency.

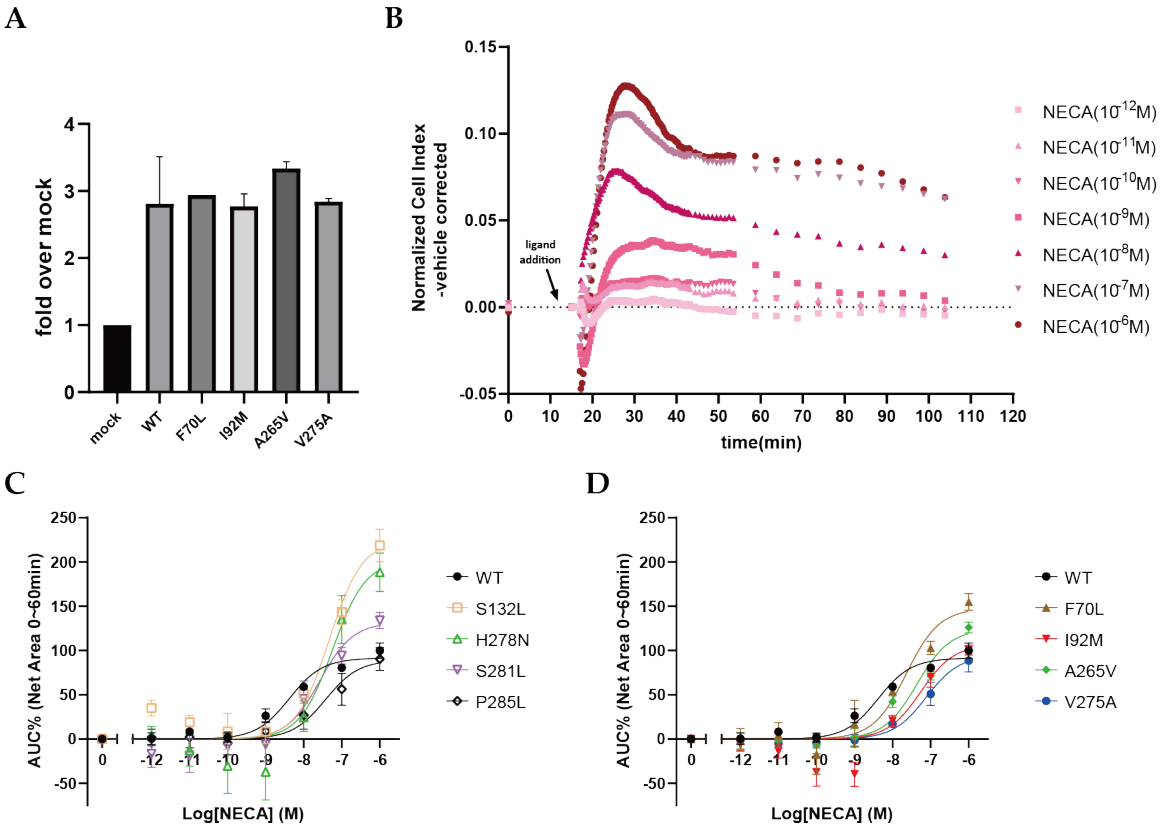

Figure 3.5. Functional characterization of wild-type and mutant A_{2A}ARs by NECA stimulation of transiently transfected HEK293T cells, using a label-free impedance based cell morphology assay. (**A**) Expression level of transiently transfected WT and mutant A_{2A}ARs on HEK293T cells, measured by enzyme-linked immunosorbent assay. Data are shown as mean ± SD of two independent experiments performed in quintuplicate. (**B**) Representative graph of vehicle-normalized cell index after stimulation with different concentrations of NECA at the wild-type A_{2A}AR. (**C, D**) Concentration-response curves of NECA for wild-type and mutant A_{2A}ARs derived from area under curve within 60 minutes after ligand addition. The response to vehicle was normalized as 0%, and the response to 1μM NECA at the wild-type receptor was set to 100%. Data are shown as mean ± SEM of three independent experiments each performed in duplicate.

Table 3.2. Potency and efficacy of NECA stimulation at the wild-type (WT) and mutant A_{2A}ARs derived from cell morphology assay.

Mutant	Potency pEC_{50} [a]	Efficacy E_{max} (%) [a]	Relative efficacy τ [b]
WT	8.4 ± 0.2	100 ± 5	37 ± 13
$F70L^{ECL1}$	7.6 ± 0.2	164 ± 19	28 ± 11
$I92M^{3.40}$	7.2 ± 0.2**	119 ± 4	10 ± 3
$A265V^{ECL3}$	7.4 ± 0.2*	135 ± 2	21 ± 8
$V275A^{7.40}$	7.1 ± 0.1**	106 ± 19	1 ± 0*
$S132L^{4.53}$	7.3 ± 0.0*	248 ± 30***	n.a.
$H278N^{7.43}$	7.3 ± 0.2**	223 ± 33**	n.a.
$S281L^{7.46}$	7.7 ± 0.3	146 ± 25	n.a.
$P285L^{7.50}$	7.4 ± 0.5*	101 ± 8	n.a.

[a] Log potency (pEC_{50}) and efficacy (E_{max}) of NECA were calculated from concentration-response curves derived from area under curve of CI changes within 60 minutes after stimulation. [b] Relative efficacy was analyzed by the operational model of Black and Leff (1983) using global fitting. n.a. = not applicable, relative efficacy could not be determined as no affinity was obtained for NECA for these mutants. Data are represented as Mean ± SEM of three independent experiments performed in duplicate. (Significant difference from wild-type was shown as *P < 0.05, **P < 0.01, ***P < 0.001, ordinary one-way ANOVA with Dunnett's multiple comparisons test).

Besides agonist-dependent activation, the inhibition of A_{2A}ARs by the antagonist ZM241385 was also investigated. Since ZM241385 often shows inverse agonism on A_{2A}AR, we first studied this pharmacological feature in the impedance-based assay. As shown in **Figure 3.6A**, after addition of 1 μM ZM241385 to HEK293T cells transfected with wild-type A_{2A}AR, the cell index first slightly increased, then sharply decreased within 5 minutes, and further decreased slowly over time. Upon normalization of the response to vehicle, the area under curve value was thus negative, indicating that ZM241385 exhibits an opposite pharmacological effect towards the agonist NECA (**Figure 3.5B**). The responses of wild-type and mutant A_{2A}ARs to 1 μM ZM241385 were quantified in **Figure 3.6B** and **Table 3.3**. Most mutants showed similar levels of inverse agonism as the wild-type A_{2A}AR. However, mutants S132L, H278N and S281L displayed a much lower level of inverse agonism compared to the wild-type A_{2A}AR. Interestingly, NECA induced a higher level of activation at these mutants (**Table 3.2**), indicating that these mutations induced a conformation of the receptor that had less basal activity, but was prone to higher levels of agonist-induced activation.

Lastly, we compared the inhibitory effects of ZM241385 on NECA-induced activation at the wild-type and different A_{2A}AR mutant receptors. A dose-dependent inhibition of ZM241385 on wild-type A_{2A}AR was observed, as shown in **Figure 3.6C**. Dose-response curves are depicted for all mutants in **Figure 3.6D** and pIC_{50} values are shown in **Table 3.3**. Compared to wild-type A_{2A}AR (pIC_{50} = 6.4 ± 0.3), ZM241385 displayed significantly higher potency at S132L (pIC_{50} = 7.3 ± 0.1), and H278N (pIC_{50} = 7.4 ± 0.1). Also, a small but significant increase in potency was found at F70L (pIC_{50} = 6.7 ± 0.2), I92M (pIC_{50} = 6.9 ± 0.1), and S281L (pIC_{50} = 6.6 ± 0.1), whereas the potency at A265V (pIC_{50} = 6.3 ± 0.2) was similar to the wild-type A_{2A}AR. However, ZM241385 was not able to inhibit NECA-induced activation at V275A and P285L, unless high

concentrations were used. Of note, its affinity was not affected at V275A (and could not be determined at P285L; **Table 3.1**), indicating that its potency was negatively impacted by these mutations.

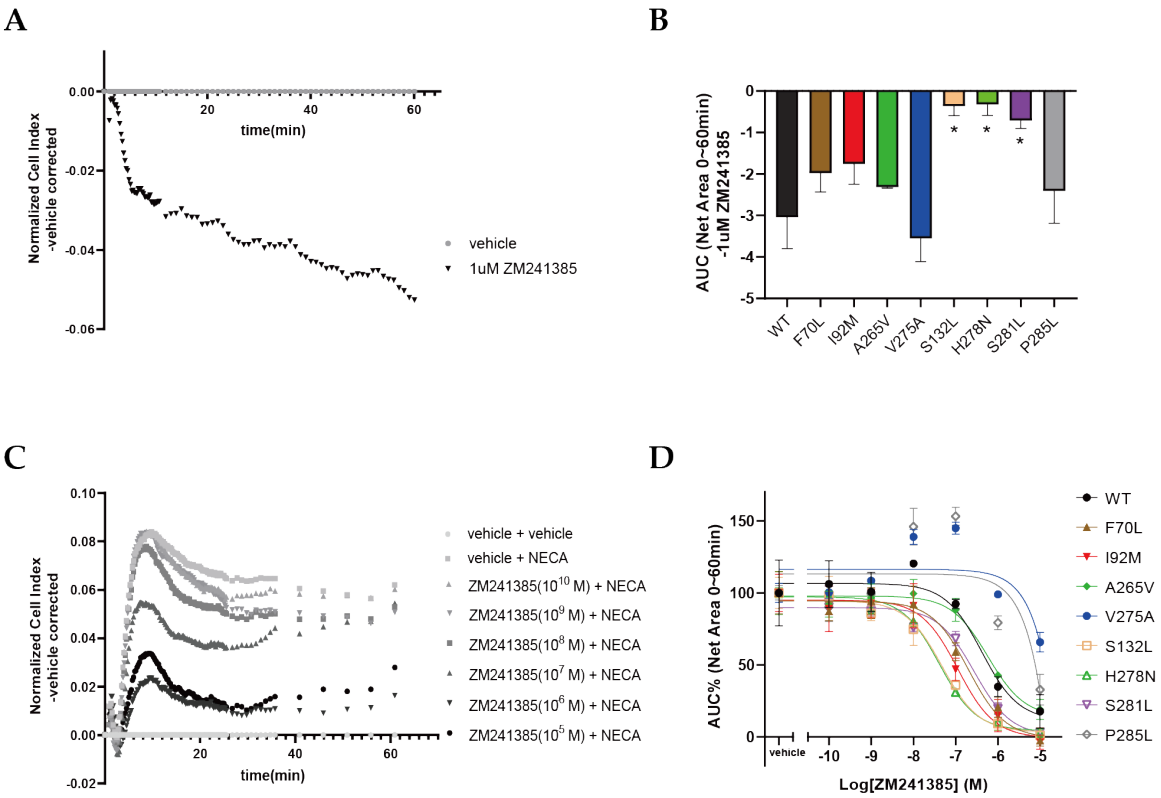

Figure 3.6. Functional characterization of wild-type and mutant A_{2A}ARs with the inverse agonist ZM241385 at transiently transfected HEK293T cells, using a label-free impedance based cell morphology assay. (**A**) A representative time-trace of normalized cell index of WT-A_{2A}AR expressing HEK293T cells stimulated with 1 µM ZM241385. (**B**) Area under the curve within 60 min after ZM241385 treatment were used to quantify its inverse agonism at A_{2A}ARs. Data are shown as mean ± SEM of three independent experiments performed in duplicate. Significant difference from WT-A_{2A}AR was shown as *P <0.05, ordinary one-way ANOVA with Dunnett's multiple comparisons test. (**C**) Representative graph of normalized cell index of different concentrations of ZM241385 on NECA-stimulated wild-type A_{2A}AR. Vehicle was used for baseline correction. (**D**) Concentration-response curves of ZM241385 for wild-type and mutant A_{2A}ARs derived from area under curve within 60 minutes after NECA addition. Response to vehicle was normalized to 0%, and response to EC_{80} of NECA after pretreatment with vehicle was normalized to 100%. Data are shown as mean ± SEM of three independent experiments each performed in duplicate.

Table 3.3. Quantification of the inverse agonism of ZM241385 at A_{2A}ARs and the inhibitory potency of ZM241385 on NECA stimulation.

Mutant	Inverse agonism of ZM241385 - 1 µM [a]	Inhibition pIC_{50} [b]
WT	-3.0 ± 0.8	6.4 ± 0.3
$F70L^{ECL1}$	-2.0 ± 0.5	6.7 ± 0.2
$I92M^{3.40}$	-1.8 ± 0.5	6.9 ± 0.1
$A265V^{ECL3}$	-2.3 ± 0.0	6.3 ± 0.2
$V275A^{7.40}$	-3.6 ± 0.6	n.d.
$S132L^{4.53}$	-0.4 ± 0.2**	7.3 ± 0.1**
$H278N^{7.43}$	-0.3 ± 0.3**	7.4 ± 0.1**
$S281L^{7.46}$	-0.7 ± 0.2*	6.6 ± 0.1
$P285L^{7.50}$	-2.4 ± 0.8	n.d.

[a] In the whole-cell based cell morphology assay, inverse agonism was calculated from area under curve of CI changes within 60 minutes after ZM241385 addition. [b] Cells were pretreated with increasing concentrations of ZM241385 before stimulating with EC_{80} of NECA. Inhibitory potency of ZM241385 (pIC_{50}) was calculated from concentration-response curves derived from area under curve of CI changes within 60 minutes after NECA addition. n.d. = not determined, as no sigmoidal inhibition curve could be obtained. Data are represented as Mean ± SEM of three independent experiments performed in duplicate. (Significant difference from wild-type was shown as *P <0.05, **P <0.01, ***P <0.001, ordinary one- way ANOVA with Dunnett's multiple comparisons test).

2.6. Structural modelling

To provide insight in the structure-activity relationship observed for the introduced mutants, we mapped each of the mutations on the available experimentally determined structures of the A_{2A}AR, for which we used the inactive (PDB ID: 4EIY), active-like (PDB ID: 2YDV) and fully active (PDB ID: 5G53) structures. As shown in **Figure 3.7A**, the mutations are scattered around the binding pocket, though some clustering can be observed of residues for instance in TM7. We focused on mutations that abominated binding and were either in direct contact with the ligand in the binding pocket, i.e. H278N, and those that introduced large changes in amino acid composition that might influence the activation of the receptor, e.g. S132L and P285L. H278 forms an extensive hydrogen bond network with the ribose moiety of the agonist (**Figure 3.7B**). These hydrogen bond patterns might be impaired by H278N mutation, which explains why the potency of NECA was significantly reduced for this mutant (**Table 3.2**). Residue P285 is located in TM7 and results in a large conformational rearrangement in the active-like structure, while the orientation of the helix in the fully active structure is closer to the inactive structure (**Figure 3.7C**). It is well known that Pro residues introduce alpha-helical kinks, which might facilitate this movement. Therefore, in P285L mutant, the substitution of Pro by Leu might abrogate this conformational rearrangement of TM7, thus resulting in decrease in the potency of both NECA and ZM241385 in impedance-based assay (**Table 3.2**, **Table3**). Although mutation S132L was also shown to greatly decrease the potency of NECA, it does not undergo any structural rearrangements when comparing the different states of crystal structure (**Figure 3.7D**), and is relatively far away from the binding site. Similarly, the S281L mutation, which also abolished binding, does not undergo large conformational rearrangements in active or inactive structures.

Thus, in both cases the mechanism of the pharmacological effects of S132L and S281L remains to be revealed.

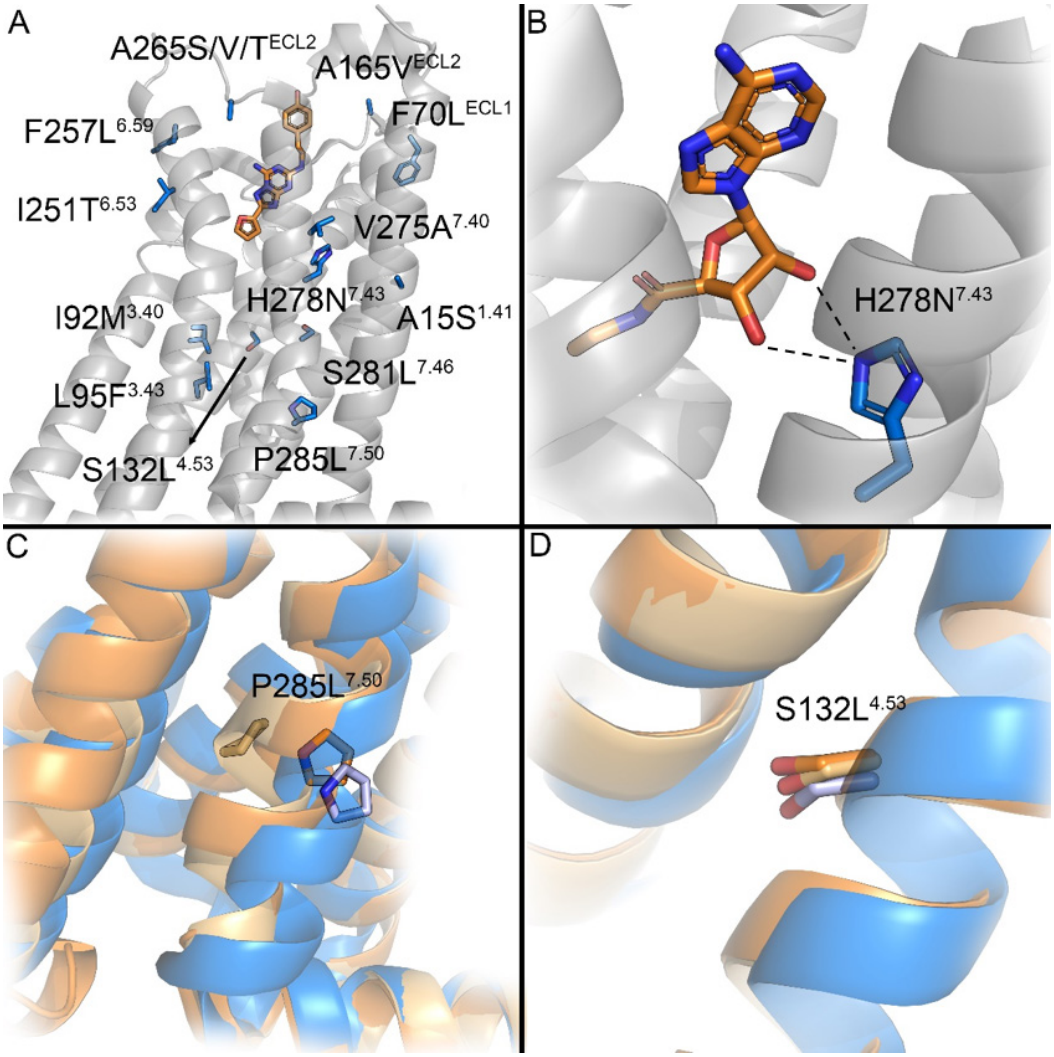

Figure 3.7. (**A**) Overview of all mutations investigated in this work, mapped on the inactive structure of the receptor (blue) the antagonist ZM241385 is shown in orange. (**B**) The residue H278 is involved in agonist binding (NECA, orange), forming hydrogen bond (dash lines) with the ribose moiety. (**C**) P285 undergoes extensive conformational rearrangement in the active-like structure (light orange). The active structure (orange) is closer to the inactive structure. (**D**) Residue S132 does not undergo extensive rearrangement compared between inactive, active-like and active structures.

3. Discussion

Mutagenesis studies in $A_{2A}AR$ have been performed since the 1990s, later on complemented by computational modeling and crystallography [26]. From these studies, numerous $A_{2A}AR$ mutations are known to alter ligand binding and receptor activation [27, 28]. In addition, it has been reported that impaired receptor expression is the most common defect caused by GPCR mutations, often combined with receptor instability and malfunction [29]. However, as $A_{2A}AR$ is emerging as a novel therapeutic target for cancer, little attention has been given to cancer-associated mutations of the receptor and their potential pharmacological effects in the context of cancer biology and targeting. Therefore, in this study 15 single site mutations of $A_{2A}AR$ were

retrieved from Genomic Data Commons Data Portal [30]. These mutations were characterized for their expression levels and effects on ligand binding and receptor function.

3.1. Some cancer-associated mutations cause a conformational change of $A_{2A}AR$

Mutations S132L$^{4.53}$ and H278N$^{7.43}$ decreased the potency of NECA over 10-fold, whereas the E_{max} was increased by more than 2-fold (**Figure 3.5C**). The decreased potency could be caused by lower receptor expression, as higher agonist concentrations were required for exerting a certain level of biological activity [31]. In addition, residue His278$^{7.43}$ is in direct contact with NECA by extensive hydrogen bonding (**Figure 3.7B**), and mutation to Asn might impair this interaction. This has also been reported in a previous study, where substitution of His278$^{7.43}$ with either Ala, Lys or Asn abolished binding of agonists NECA, CGS21680 and antagonist XAC [28]. Since S132L$^{4.53}$ is located relatively far away from the binding site (**Figure 3.7A**), the decreased potency may not result from a change in ligand binding. Moreover, the effect of this mutation might be caused by an overall destabilization of the receptor as suggested by a much lower receptor expression. Further studies are needed to clarify the structural basis of altered receptor function by S132L$^{4.53}$, which currently is the mutation with the highest incidence among all cancer-associated $A_{2A}AR$ mutations in the GDC Data Portal. Interestingly, these two mutations not only increased the E_{max}, but also drastically decreased the level of inverse agonism by ZM241385 (**Figure 3.6B**, **Table 3.3**), showing less constitutive activity of the receptor and thus suggesting a more inactive conformation of the receptor. Constitutive activity of the $A_{2A}AR$ has been reported before, where $A_{2A}AR$ was found to display a native level of activation in the absence of any agonist, and inverse agonists bound preferentially to the inactive state to reduce the activity [32, 33]. In addition, in comparison to the wild-type receptor, the potency of ZM241385 at S132L$^{4.53}$ and H278N$^{7.43}$ was not impaired, but actually increased (**Figure 3.6**, **Table 3.3**). Therefore, it seems that S132L$^{4.53}$ and H278N$^{7.43}$ shift the conformational equilibrium of $A_{2A}AR$ towards the inactive state. However, this shift cannot be observed in our static structure analysis, but can be modelled with more advanced methods, for example free energy simulation [34]. Of note, Gao *et al.* have reported a sodium binding pocket in $A_{2A}AR$ formed by His278$^{7.43}$ and Glu13$^{1.39}$, and showed that mutation H278Y$^{7.43}$ reduced the negative allosteric effect of sodium ions on agonist binding [35]. Although a physiological concentration of NaCl was found to be sufficient to stabilize the inactive conformation of the $A_{2A}AR$ [36], it remains unknown whether substitution of His278$^{7.43}$ with Asn instead of Tyr would augment the allosteric effect of sodium ions to achieve this effect.

S281$^{7.46}$ has also been investigated in other mutagenesis studies, where Kim *et al.* found that substitution of Ser by Ala abolished binding of agonist GGS21680 and antagonist XAC, while substitution to Thr increased the affinity of NECA, GGS21680 and XAC [27]. Besides, Jiang *et al.* reported that substitution of Ser281$^{4.53}$ by Asn increased the affinity of NECA and CGS21680, but decreased the affinity of ZM241385 [37]. These studies suggest that the hydrophilic side chain of S281$^{7.46}$ is beneficial to ligand recognition. Therefore, it is inferred that the hydrophobic mutation S281L$^{7.46}$ would cause a decrease in affinity of NECA, consistent with the slightly decreased potency observed in the cell morphology assay. Moreover, we observed that mutation S281L$^{7.46}$ decreased the inverse agonism induced by ZM241385, indicating a more inactive conformation of the receptor.

P285$^{7.50}$ is located in the highly conserved NPxxY motif that is known to be involved in GPCR activation [2, 38]. Massink *et al.* found that mutation N284A$^{7.49}$ in $A_{2A}AR$ completely abolished receptor activation [39]. However, in our study, mutation P285L$^{7.50}$ caused a 10-fold decrease in

potency of NECA, but similar efficacy at the wild-type $A_{2A}AR$, indicating that activation of the receptor was also impaired albeit not abolished. Based on structural modeling (**Figure 3.7C**), $P285^{7.50}$ shows a drastic conformational rearrangement during the receptor activation process, which might be impeded if Pro is substituted by Leu. Interestingly, ZM241385 could only inhibit the activation of $P285L^{7.50}$ mutant at concentrations above 1 μM (**Figure 3.6D**). Although the affinity of ligands at $P285L^{7.50}$ could not be determined, it has been reported that mutation $P285C^{7.50}$ in A_1AR slightly increases the affinity of its antagonist DPCPX [40]. As $Pro^{7.50}$ cannot act as hydrogen-bond donor and is conserved among GPCRs, we hypothesize that mutation $P285L^{7.50}$ could facilitate the formation of a hydrogen bond between the amino of Leu with NECA, and thus increase its affinity. This hypothesis is consistent with a significantly decreased potency of antagonist ZM241385, since competitive binding between the agonist NECA and antagonist ZM241385 might be affected by this mutation and result in altered receptor inhibition. At last, compared with wild-type $A_{2A}AR$, $P285L^{7.50}$ displayed similar E_{max} of NECA and similar inverse agonism of ZM241385, so the conformational equilibrium seems not influenced.

3.2. Some cancer-associated mutations affect ligand binding and functioning of $A_{2A}AR$

Looking into the structural feature of these mutations and their effects on ligand binding, we found that all mutations located in the extracellular loops played a role. For example, $F70L^{ECL1}$ decreased the affinity of NECA by around 4-fold, and $A165V^{ECL2}$ slightly decreased the affinity of ZM241385 and NECA, while $A265V^{ECL3}$ drastically decreased the affinity of both ligands. Besides, although these three mutations all preserved the hydrophobic side chain, they still showed a considerable impact on affinity, possibly due to an increase in steric hindrance during ligand entry. Note that, three different mutations were found at $Ala265^{ECL3}$, i.e. A265S, A265V and A265T, and is located next to $His264^{ECL3}$, which is part of the orthosteric binding pocket of $A_{2A}AR$. $His264^{ECL3}$ has been shown to make an aromatic interaction with the 4-hydroxyphenyl ring of ZM241385 [41]. Guo *et al.* have also reported a hydrogen bond network formed by $His264^{ECL3}$, $Glu169^{ECL2}$ and $Thr256^{6.58}$ with ZM241385, and disruption of this network by mutation of either of these residues decreased the binding affinity of ZM241385 due to a faster dissociation rate of the antagonist from the receptor [18]. These studies are in line with our findings that the introduction of bulkier hydrophobic side chain at Ala265 by substitution with a Valine might cause stronger steric hindrance to His264, and thus a loss in affinity of the antagonist.

Of further interest is the mutations' effects on receptor function. For $F70L^{ECL1}$, $I92M^{3.40}$, and $A265V^{ECL3}$, a decreased potency for NECA was observed (**Figure 3.5D**, **Table 3.2**), which was correlated to a decreased binding affinity of this agonist (**Figure 3.4A**, **Table 3.1**). However, the decrease in potency for $I92M^{3.40}$ was larger than for $F70L^{ECL1}$ and $A265V^{ECL3}$, resulting in a lower relative efficacy. The relative efficacy τ reflects the ability of a specific agonist to activate the receptor in relation to its receptor occupancy level (so more system independent) [42]. When τ is large, resulting from an agonist with a much higher potency than its affinity and with 100% E_{max}, this indicates full agonism. *Vice versa*, a small τ or lower E_{max} indicates partial agonism. As such, although the apparent maximal response to NECA of $V275A^{7.40}$ was similar to that of wild-type $A_{2A}AR$ (**Figure 3.5D**, **Table 3.2**), when calculating its relative efficacy, NECA seems to act as a partial agonist. $V275A^{7.40}$ is the only mutation that increased the affinity of NECA but decreased its potency. In other words, activation of this mutant receptor by NECA is dependent on a larger proportion of receptor occupancy, and thus indicates a loss in coupling efficiency to the intracellular signaling pathways. Similar effects have been described for VEGFR and β

adrenergic receptors, where agonists may show "pluridimensional efficacy" depending on the level of receptor expression, the cell background and signaling pathway observed [43, 44]. This and our data substantiates the importance of calculating relative efficacies when comparing agonists and receptor variants, especially when using a (transient) heterologous expression systems. What's more, ZM241385 could only exert inhibitory effects on V275A$^{7.40}$ at high concentrations (**Figure 3.6D**, **Table 3.3**), resulting from the increased affinity of NECA and unaffected affinity of ZM241385 (**Figure 3.4B**, **Table 3.1**), which follows the same pattern as P285L$^{7.50}$. Importantly, the lost potency of prototypic drug ZM241385 at these two mutations indicates that they could be problematic in cancer treatment and deserve follow-up studies.

3.3. Conclusions

In this chapter, we characterized 15 cancer-associated mutations of the human adenosine A_{2A} receptor for their effects on ligand binding and receptor function in HEK293T cells. Several mutations were found to affect binding affinity of an agonist or antagonist, receptor expression level, constitutive activity of the receptor, as well as receptor activation and inhibition by a reference agonist and antagonist, respectively. This study provides novel fundamental insights into the structure-activity relationship of the adenosine A_{2A} receptor. Based on these findings, further studies in cancer cell models are required to reveal the role of these A_{2A}AR mutations in cancer progression. Moreover, identifying antagonists that affect wild-type as well as mutant receptors may lead to optimized therapeutic strategies targeting A_{2A}AR.

4. Materials and Methods

4.1. Chemicals and Reagents

[^{3}H]ZM241385 (specific activity 50 Ci/mmol) was purchased from American Radiolabeled Chemicals Inc. (St. Louis, USA). Unlabeled ZM241385, 5′-Nethylcarboxamidoadenosine (NECA) and adenosine deaminase (ADA) were purchased from Merck Life Science N.V. (Amsterdam, the Netherlands). BCA protein assay reagent was obtained from Fisher Scientific (Landsmeer, the Netherlands). Quick Change II Site-Directed Mutagenesis Kit was purchased from Agilent Technologies Netherlands B.V. (Amstelveen, the Netherlands). All other chemicals were of analytical grade and obtained from standard commercial sources.

4.2. Site-Directed Mutagenesis

Plasmid DNA of A_{2A}AR mutants were constructed by polymerase chain reaction (PCR) based on pcDNA3.1(-)-A_{2A}AR-wt with N-terminal FLAG tag and C-terminal His tag as template, using Quick Change II Site-Directed Mutagenesis Kit. Mutagenesis primers for PCR cloning were designed using the online Quickchange primer design tool (Agilent Technologies) and synthesized by Integrated DNA Technologies (Coralville, USA). All DNA sequences were verified by Sanger sequencing at Leiden Genome Technology Center (Leiden, the Netherlands).

4.3. Cell culture and transfection

Human embryonic kidney 293T (HEK293T) cells were grown in Dulbecco's modified Eagle's medium (high glucose) supplemented with 10% fetal calf serum, 200 µg/ml penicillin, 200 µg/ml streptomycin, at 37°C and 5% CO_2. Cells were subcultured at a ratio of 1:15 twice a week on 10 cm ø plates. Before transfection, cells were subcultured at a ratio of 1:8, and after 24 hours proliferation they could reach ~50% confluency. Cells were transfected with the wild-type or mutant pcDNA3.1(-)-A_{2A}AR plasmid DNA (1 µg/plate) using the calcium phosphate precipitation method [45]. In short, 1 µg plasmid DNA was dissolved in 365 µl water, then mixed

with 135 µl 1M $CaCl_2$ solution. The mixture was added dropwise to HBSS buffer while aeration to form a fine precipitate, which was applied 1 ml/plate to HEK293T cells.

4.4. Enzyme-linked Immunosorbent assay (ELISA)

To determine the expression level of wild-type or mutant A_{2A}ARs on HEK293T cell membrane, 24 hours after transfection, cells were detached with PBS/EDTA and resuspended in culture medium. Cells were then seeded in poly-D-lysine coated 96-well plate at a density of 1×10^6 cells/well in quintuplicate. After 24 hours incubation at 37°C and 5% CO_2, medium were removed and cells were washed with PBS and subsequently fixed with 100 µl/well 4% formaldehyde for 10 minutes. Cells were washed with TBS twice before adding 100 µl/well blocking buffer (2% w/v bovine serum albumin in TBST) and incubated for 30 minutes at room temperature. After that, blocking buffer was removed and cells were incubated in 100 µl/well primary antibody (mouse anti-FLAG monoclonal antibody, Sigma F3165, 1:4000) for 2 hours at room temperature while shaking at 300rpm. Next, primary antibody was removed and cells were washed with TBST three times before addition of 100 µl/well secondary antibody (goat anti-mouse IgG HRP-conjugated, Jackson ImmunoResearch Laboratories 115-035-003, 1:10000) and incubated for 1 hour at room temperature while shaking. After removal of the secondary antibody, cells were washed three times with TBS. Next, cells were treated with 100 µl/well 3, 3', 5, 5'-tetramethylbenzidine (TMB, Sigma T0440) for 5 minutes in dark, then the reaction was stopped by addition of 100 µl/well 1 M H_3PO_4 solution. Immediately after that, the absorbance was measured at 450 nm using EnVision™ microplate reader. HEK293T cells transfected with vector pcDNA3.1 plasmid were used as a control (mock), of which the absorbance value was normalized at 1 for data analysis.

4.5. Membrane preparation and determination of specific [^{3}H]ZM241385 binding

Preparation of cell membranes over-expressing A_{2A}ARs for radioligand binding assays were performed as reported previously[18]. Briefly, HEK293T transiently expressing wild-type or mutant A_{2A}AR were detached by scraping into PBS. Cell pellets were collected by centrifugation at 1000 rpm for 10 min to remove PBS, and re-suspended in ice-cold Tris-HCl buffer (50 mM, PH=7.4) prior to homogenization. The homogenized suspensions were centrifuged at 100,000 × g for 20 min at 4 °C, and re-suspended in Tris-HCl buffer to repeat the homogenization-centrifugation cycle again. At last, membranes from ten 10 cm ø plates were re-suspended in 1 ml of assay buffer (50 mM Tris-HCl, 5 mM $MgCl_2$, 0.1% CHAPS) as used in radioligand binding assays, homogenized, and treated with adenosine deaminase (0.8 IU/ml) to degrade endogenous adenosine. Membranes were stored in 100-250 µl aliquots at -80 °C. Membrane protein concentrations were determined using the BCA method [46].

To determine the binding capacity of [^{3}H]ZM241385 with A_{2A}ARs, 25 µl membrane (10 µg protein/well) were mixed in a total volume of 100 µl, with the presence of 2.5 nM [^{3}H]ZM241385, with 100 µM NECA to determine non-specific binding (NSB) or without NECA to determine total binding (TB). The mixtures were incubated at 4°C for 2 hours while shaking at 200 rpm. Incubation was terminated by rapid vacuum filtration to separate the bound and free radioligand through 96-well GF/C filter using Filtermate-harvester (PerkinElmer, Groningen, Netherlands). Filters were washed ten times with ice-cold wash buffer (50 mM Tris-HCl, 5 mM $MgCl_2$) before drying at 55°C oven for 30 minutes. To measure the membrane-bound radioactivity, 25ul MicroScint™-20 cocktail was added to each well, and the filter was measured by MicroBeta^2 Microplate Counter (PerkinElmer, Groningen, Netherlands).

4.6. Radioligand homologous and heterologous displacement assays

For the homologous displacement assay, increasing concentrations (10^{-12} M to 10^{-6} M) of unlabeled ZM241385 were used to displace binding of three concentrations of [^{3}H]ZM241385, i.e. 0.5 nM, 1nM, 2.5 nM, which were distributed around the estimated K_D of ZM241385 with A_{2A}AR. For the heterologous displacement assay, increasing concentrations (10^{-11} M to 10^{-5} M) of NECA were used to displace binding of 2.5 nM [^{3}H]ZM241385. Based on the pre-determined [^{3}H]ZM241385 binding capacity at the different mutants, 25 µl membrane aliquots containing 1~20 µg protein were used to adjust the total binding with 2.5 nM [^{3}H]ZM241385 to approximately 2000 dpm, and non-specific binding less than 10% of total binding. Membranes were incubated with the radioligand and the compound of interest in a total volume of 100 µl assay buffer (50 mM Tris-HCl, 5 mM $MgCl_2$, 0.1% CHAPS), as described above.

4.7. Label-free whole-cell assay (xCELLigence RTCA system)

Functional characterization of transient transfected wild-type and mutant A_{2A}ARs was performed on HEK293T cells, with the xCELLigence RTCA system as described previously [47]. Briefly, an arrayed microelectrode is embedded at the bottom of each well of a 96-well E-plate (Roche Applied Science, Mannheim, Germany). During cell spreading and proliferation, the cell morphology changes will affect the electronic readout of cell-sensor impedance (Z), which is monitored in real time by the xCELLigence RTCA system and displayed as the cell index (CI). If the cells are stimulated by a ligand, the changes in CI will reflect the overall cellular response upon activation of GPCR-mediated signaling.

To study the stimulation of A_{2A}ARs by NECA, HEK293T cells were transfected with wild-type or mutant A_{2A}AR following the methods described above. 24 hours after transfection, cells were detached with PBS/EDTA and suspended with culture medium. Cell suspension was centrifuged at 1000 rpm for 5 min to remove the supernatant, then cell pellets were re-suspended in culture medium to adjust the concentration to 1×10^6 cells/ml. First, 50 µl culture medium was added to each well of a 96-well E-plate to measure the background (Z_0). Next, 40 µl of cell suspension containing 40,000 cells was added to each well and E-plate was left at room temperature for 30 min before being placed on the recording device station in the incubator at 37°C and 5% CO_2. The cells were cultured for 17~20 h until the end of log phase, during which CI was continuously measured every 15 min. After that, 5ul adenosine deaminase solution (ADA, 2.5 IU/ml) was added to each well and incubated for 1.5 h to remove the adenosine present in culture medium. Subsequently, cells were stimulated with 5 µl NECA (final concentration ranges from 10^{-12} M to 10^{-6} M) or vehicle control (final concentration of 0.1% DMSO). The changes in CI after agonist addition were measured every 15 s within the first 30 min, followed by every 5 min up to 120 min. For data analysis, CI of each group was normalized by subtracting the baseline (vehicle control) to correct for any non-specific signals. Dose response curves were generated from the area under curve (AUC) within the first 60 min after agonist addition, and parameters including EC_{50}, EC_{80} and E_{max} were calculated to describe the potency and efficacy of NECA stimulation at wild-type or mutant A_{2A}ARs.

To characterize the pharmacological effects of ZM241385 at wild-type or mutant A_{2A}ARs, the experiments were performed similar as described above. Cells were then treated with 5 µl ZM241385 (final concentration ranges from 10^{-10} M to 10^{-5} M) or vehicle control (final concentration of 0.05% DMSO), and changes in CI were measured every 15 s within the first 10 min and every 1 min up to 90 min. After that, 5 µl NECA (final concentration equals to the EC_{80} of NECA for each A_{2A}AR variant) or vehicle control (final concentration of 0.05% DMSO) was

added to each well. For data analysis, CI of each group was normalized by subtracting the baseline (vehicle control) to correct for any non-specific signals. AUC within 60 min after compound addition were used to describe the initial response of ZM241385 itself and the inhibitory effects of ZM241385 on NECA stimulation.

4.8. Data analysis

All experimental data were analyzed using GraphPad Prism 9.0 (GraphPad Software Inc., San Diego, CA) and values obtained were means of two or three independent experiments. K_D values of [^{3}H]ZM241385 obtained from homologous displacement assays were calculated using nonlinear regression curve fitting (Binding-Competitive-One site-Homologous), where 3 concentrations of [^{3}H]ZM241385 were input and K_D was obtained by global fitting. B_{max} values were obtained from homologous displacement assays in "dpm", and converted to pmol/mg using equations:

$$\boldsymbol{B_{max}\,(Ci)} = \frac{\boldsymbol{Bmax\,(dpm)}}{\boldsymbol{2.22 * 10^{-12}}}$$

$$\boldsymbol{B_{max}\,(mmol)} = \boldsymbol{B_{max}\,(Ci)/Specific\ activity\,(Ci/mmol)}$$

$$\boldsymbol{Specific\ activity} = \boldsymbol{Specific\ activity\ at\ t_0} * \boldsymbol{0.5}^{\frac{\boldsymbol{time\ lapse\ since\ prodection\ date}}{\boldsymbol{half\ life\ of\ radio\ label}}}$$

$$\boldsymbol{B_{max}\,(pmol/mg)} = \frac{\boldsymbol{B_{max}\,(mmol) * 10^9}}{\boldsymbol{Amout\ of\ membrane\ protein\ per\ well\,(mg)}}$$

IC_{50} values obtained from heterologous displacement assays were calculated by nonlinear regression curve fitting using a one-site competitive binding model, where K_D values were taken from homologous displacement assay for each receptor variant, and K_i were converted from IC_{50} following the Cheng-Prusoff equation [48]:

$$\boldsymbol{K_i} = \frac{\boldsymbol{IC_{50}}}{\boldsymbol{1} + \frac{\boldsymbol{[Radioligand]}}{\boldsymbol{K_D}}}$$

EC_{50} and E_{max} values in cell morphology assay were obtained by plotting the normalized CI traces using RTCA Software 2.0 (Roche Applied Science). Dose-response curves were generated by calculating the area under curve over the first 60 minutes after compound addition, and analyzed using nonlinear regression fitting (three parameters model) to determine the EC_{50} and E_{max}. Relative efficacies (τ) of agonist at each receptor variant were obtained by fitting the data to the operational model of Black and Leff [49], which correlates the biological effect E with agonist concentration [*A*]:

$$\boldsymbol{E} = \frac{\boldsymbol{E_{max} \cdot \tau \cdot [A]}}{\boldsymbol{K_D + (\tau + 1) \cdot [A]}}$$

4.9. Modelling

Figures were created based on the experimentally determined structures for the A_{2A}AR crystal structures, with PDB codes 4EIY [15] for the inactive, 2YDV [14] for the active like and 5G53 [50] for the fully active structure. Figures were generated using the PyMOL Molecular Graphics System version 2.0 (Schrödinger, LLC., USA).

Supplementary information

Table S3.1. List of cancer-associated A_{2A}AR mutations investigated in this study.

Mutation	Affected cases per cancer type across the GDC	Cancer type
A15S$^{1.41}$	1/987	Breast invasive carcinoma
F70L^{ECL1}	1/533	Uterine Corpus Endometrial Carcinoma
I92M$^{3.40}$	1/1060	Lung adenocarcinoma
L95F$^{3.43}$	1/1060	Lung squamous cell carcinoma
S132L$^{4.53}$	3/533 1/399	Uterine Corpus Endometrial Carcinoma (3 cases) Colon adenocarcinoma (1 case)
A165V^{ECL2}	1/399	Colon adenocarcinoma
I251T$^{6.53}$	1/399	Colon adenocarcinoma
F257L$^{6.59}$	1/533	Uterine Corpus Endometrial Carcinoma
A265S^{ECL3}	1/987	Breast invasive carcinoma
A265V^{ECL3}	1/987	Breast invasive carcinoma
*A265T^{ECL3}	1/1060	Lung squamous cell carcinoma
V275A$^{7.40}$	1/533	Uterine Corpus Endometrial Carcinoma
H278N$^{7.43}$	1/399	Colon adenocarcinoma
*S281L$^{7.46}$	1/533 1/79	Uterine Corpus Endometrial Carcinoma (1 case) Rectum adenocarcinoma (1 case)
P285L$^{7.50}$	1/1060	Lung squamous cell carcinoma

Mutations are shown in the numbering of A_{2A}AR amino acid sequence as well as the Ballesteros and Weinstein number in superscript. * A_{2A}AR Mutations that were also identified as natural variants.

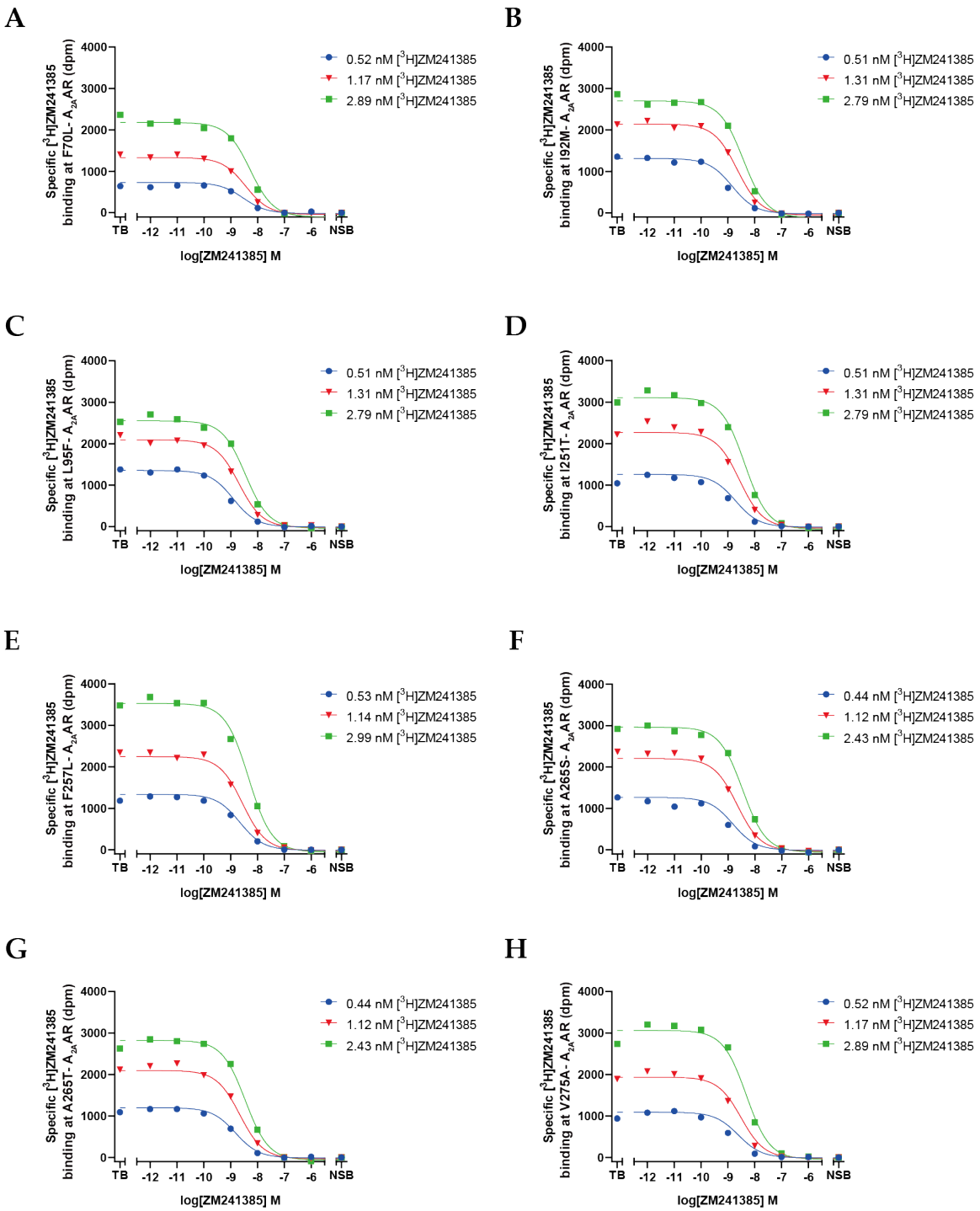

Figure S3.1. Homologous displacement of three concentrations of [^{3}H]ZM241385 by increasing concentrations of ZM241385 at mutant A_{2A}ARs. Different concentrations of membranes were used dependent on receptor expression levels: (**A**) F70L-A_{2A}AR (4.5 µg); (**B**) I92M-A_{2A}AR (4 µg); (**C**) L95F-A_{2A}AR (3 µg); (**D**) I251T-A_{2A}AR (3 µg); (**E**) F257L-A_{2A}AR (1.5 µg); (**F**) A265S-A_{2A}AR (1.5 µg); (**G**) A265T-A_{2A}AR (1 µg); (**H**) V275A-A_{2A}AR (2 µg). Representative curves from one experiment performed in duplicate.

References

1. Fredholm, B.B., et al., *International Union of Pharmacology. XXV. Nomenclature and classification of adenosine receptors.* Pharmacol Rev, 2001. **53**(4): p. 527-52.
2. Trzaskowski, B., et al., *Action of molecular switches in GPCRs-theoretical and experimental studies.* Current medicinal chemistry, 2012. **19**(8): p. 1090-1109.
3. de Lera Ruiz, M., Y.H. Lim, and J. Zheng, *Adenosine A_{2A} receptor as a drug discovery target.* J Med Chem, 2014. **57**(9): p. 3623-50.
4. Blay, J., T.D. White, and D.W. Hoskin, *The extracellular fluid of solid carcinomas contains immunosuppressive concentrations of adenosine.* Cancer Res, 1997. **57**(13): p. 2602-5.
5. Kroemer, G., et al., *Immunogenic Cell Death in Cancer Therapy.* Annual Review of Immunology, 2013. **31**(1): p. 51-72.
6. Cekic, C. and J. Linden, *Adenosine A_{2A} receptors intrinsically regulate CD8+ T cells in the tumor microenvironment.* Cancer research, 2014. **74**(24): p. 7239-7249.
7. Novitskiy, S.V., et al., *Adenosine receptors in regulation of dendritic cell differentiation and function.* Blood, The Journal of the American Society of Hematology, 2008. **112**(5): p. 1822-1831.
8. Young, A., et al., *A_{2A}R adenosine signaling suppresses natural killer cell maturation in the tumor microenvironment.* Cancer Research, 2018. **78**(4): p. 1003-1016.
9. Ohta, A., et al., *A2A adenosine receptor protects tumors from antitumor T cells.* Proceedings of the National Academy of Sciences, 2006. **103**(35): p. 13132-13137.
10. Beavis, P.A., et al., *Blockade of A_{2A} receptors potently suppresses the metastasis of CD73+ tumors.* Proceedings of the National Academy of Sciences, 2013. **110**(36): p. 14711-14716.
11. Young, A., et al., *Co-inhibition of CD73 and A_{2A}R adenosine signaling improves anti-tumor immune responses.* Cancer cell, 2016. **30**(3): p. 391-403.
12. Congreve, M., et al., *Targeting adenosine A_{2A} receptor antagonism for treatment of cancer.* Expert Opin Drug Discov, 2018. **13**(11): p. 997-1003.
13. Jaakola, V.-P., et al., *The 2.6 angstrom crystal structure of a human A_{2A} adenosine receptor bound to an antagonist.* Science, 2008. **322**(5905): p. 1211-1217.
14. Lebon, G., et al., *Agonist-bound adenosine A 2A receptor structures reveal common features of GPCR activation.* Nature, 2011. **474**(7352): p. 521-525.
15. Liu, W., et al., *Structural basis for allosteric regulation of GPCRs by sodium ions.* Science, 2012. **337**(6091): p. 232-236.
16. Zhukov, A., et al., *Biophysical mapping of the adenosine A_{2A} receptor.* J Med Chem, 2011. **54**(13): p. 4312-23.
17. Kooistra, A.J., et al., *GPCRdb in 2021: integrating GPCR sequence, structure and function.* Nucleic Acids Research, 2021. **49**(D1): p. D335-D343.
18. Guo, D., et al., *Molecular Basis of Ligand Dissociation from the Adenosine A_{2A} Receptor.* Mol Pharmacol, 2016. **89**(5): p. 485-91.
19. Segala, E., et al., *Controlling the Dissociation of Ligands from the Adenosine A_{2A} Receptor through Modulation of Salt Bridge Strength.* J Med Chem, 2016. **59**(13): p. 6470-9.
20. O'Hayre, M., et al., *The emerging mutational landscape of G proteins and G-protein-coupled receptors in cancer.* Nat Rev Cancer, 2013. **13**(6): p. 412-24.
21. Wu, V., et al., *Illuminating the Onco-GPCRome: Novel G protein-coupled receptor-driven oncocrine networks and targets for cancer immunotherapy.* J Biol Chem, 2019. **294**(29): p. 11062-11086.
22. Jensen, M.A., et al., *The NCI Genomic Data Commons as an engine for precision medicine.* Blood, 2017. **130**(4): p. 453-459.
23. Bongers, B.J., et al., *Pan-cancer in silico analysis of somatic mutations in G-protein coupled receptors: The effect of evolutionary conservation and natural variance.* bioRxiv, 2021: p. 2021.10.25.465693.
24. Ballesteros, J.A. and H. Weinstein, *Integrated methods for the construction of three-dimensional models and computational probing of structure-function relations in G protein-coupled receptors*, in *Receptor Molecular Biology*, S.C. Sealfon, Editor. 1995, Academic Press. p. 366-428.
25. Consortium, G.P., *A global reference for human genetic variation.* Nature, 2015. **526**(7571): p. 68.
26. Jespers, W., et al., *Structural mapping of adenosine receptor mutations: ligand binding and signaling mechanisms.* Trends in pharmacological sciences, 2018. **39**(1): p. 75-89.

27. Kim, J., et al., *Site-directed mutagenesis identifies residues involved in ligand recognition in the human A2a adenosine receptor.* J Biol Chem, 1995. **270**(23): p. 13987-97.
28. Jiang, Q., et al., *Mutagenesis Reveals Structure–Activity Parallels between Human A_{2A} Adenosine Receptors and Biogenic Amine G Protein-Coupled Receptors.* Journal of Medicinal Chemistry, 1997. **40**(16): p. 2588-2595.
29. Stoy, H. and V.V. Gurevich, *How genetic errors in GPCRs affect their function: possible therapeutic strategies.* Genes & diseases, 2015. **2**(2): p. 108-132.
30. Grossman, R.L., et al., *Toward a shared vision for cancer genomic data.* New England Journal of Medicine, 2016. **375**(12): p. 1109-1112.
31. Jakubík, J., et al., *Applications and limitations of fitting of the operational model to determine relative efficacies of agonists.* Scientific Reports, 2019. **9**(1): p. 4637.
32. Bennett, K.A., et al., *Pharmacology and structure of isolated conformations of the adenosine A_{2A} receptor define ligand efficacy.* Molecular pharmacology, 2013. **83**(5): p. 949-958.
33. Ibrisimovic, E., et al., *Constitutive activity of the A_{2A} adenosine receptor and compartmentalised cyclic AMP signalling fine-tune noradrenaline release.* Purinergic Signal, 2012. **8**(4): p. 677-92.
34. Jespers, W., et al., *Deciphering conformational selectivity in the A_{2A} adenosine G protein-coupled receptor by free energy simulations.* PLoS computational biology, 2021. **17**(11): p. e1009152.
35. Gao, Z.-G., et al., *Site-directed mutagenesis studies of human A_{2A} adenosine receptors: Involvement of glu13 and his278 in ligand binding and sodium modulation.* Biochemical Pharmacology, 2000. **60**(5): p. 661-668.
36. Gutiérrez-de-Terán, H., et al., *The role of a sodium ion binding site in the allosteric modulation of the A(2A) adenosine G protein-coupled receptor.* Structure, 2013. **21**(12): p. 2175-85.
37. Jiang, Q., et al., *Hydrophilic side chains in the third and seventh transmembrane helical domains of human A_{2A} adenosine receptors are required for ligand recognition.* Mol Pharmacol, 1996. **50**(3): p. 512-21.
38. Nygaard, R., et al., *Ligand binding and micro-switches in 7TM receptor structures.* Trends in pharmacological sciences, 2009. **30**(5): p. 249-259.
39. Massink, A., et al., *Sodium ion binding pocket mutations and adenosine A_{2A} receptor function.* Molecular pharmacology, 2015. **87**(2): p. 305-313.
40. Dawson, E.S. and J.N. Wells, *Determination of amino acid residues that are accessible from the ligand binding crevice in the seventh transmembrane-spanning region of the human A1 adenosine receptor.* Molecular Pharmacology, 2001. **59**(5): p. 1187-1195.
41. Jaakola, V.P., et al., *Ligand binding and subtype selectivity of the human A(2A) adenosine receptor: identification and characterization of essential amino acid residues.* J Biol Chem, 2010. **285**(17): p. 13032-44.
42. Black, J.W., et al., *An operational model of pharmacological agonism: the effect of E/[A] curve shape on agonist dissociation constant estimation.* British journal of pharmacology, 1985. **84**(2): p. 561-571.
43. Peach, C.J., et al., *Molecular pharmacology of VEGF-A isoforms: binding and signalling at VEGFR2.* International journal of molecular sciences, 2018. **19**(4): p. 1264.
44. Galandrin, S. and M. Bouvier, *Distinct signaling profiles of β1 and β2 adrenergic receptor ligands toward adenylyl cyclase and mitogen-activated protein kinase reveals the pluridimensionality of efficacy.* Molecular pharmacology, 2006. **70**(5): p. 1575-1584.
45. Sambrook, J., *Molecular cloning : a laboratory manual*. 2nd ed. ed, ed. E.F. Fritsch, T. Maniatis, and N. Ford. 1989: Cold Spring Harbor, N.Y. : Cold Spring Harbor Laboratory Press.
46. Smith, P.K., et al., *Measurement of protein using bicinchoninic acid.* Analytical Biochemistry, 1985. **150**(1): p. 76-85.
47. Yu, N., et al., *Real-time monitoring of morphological changes in living cells by electronic cell sensor arrays: an approach to study G protein-coupled receptors.* Anal Chem, 2006. **78**(1): p. 35-43.
48. Yung-Chi, C. and W.H. Prusoff, *Relationship between the inhibition constant (KI) and the concentration of inhibitor which causes 50 per cent inhibition (I50) of an enzymatic reaction.* Biochemical Pharmacology, 1973. **22**(23): p. 3099-3108.
49. Black, J.W. and P. Leff, *Operational models of pharmacological agonism.* Proc R Soc Lond B Biol Sci, 1983. **220**(1219): p. 141-62.
50. Carpenter, B., et al., *Structure of the adenosine A_{2A} receptor bound to an engineered G protein.* Nature, 2016. **536**(7614): p. 104-107.